Journal of Power Sources 232 (2013) 152–158

Contents lists available at SciVerse ScienceDirect

Journal of Power Sources

journal homepage: www.elsevier.com/locate/jpowsour

Short communication

One-pot synthesis of carbon coated-SnO_2/graphene-sheet nanocomposite with highly reversible lithium storage capability

Jianli Cheng [a], Huolin Xin [b], Haimei Zheng [b], Bin Wang [a,*]

[a] Environmental Energy Technologies Division, Lawrence Berkeley National Laboratory, Berkeley, CA 94720, USA
[b] Materials Sciences Division, Lawrence Berkeley National Laboratory, Berkeley, CA 94720, USA

HIGHLIGHTS

- SnO_2-C/GNS nanocomposite was synthesized by a one-pot hydrothermal approach.
- Strong oxidation and reduction process to produce GNS by Hummer's method is avoided.
- It exhibits excellent high-rate capability and cycling stability as anode material.
- The improved performance was attributed to the double carbon buffering matrix.

ARTICLE INFO

Article history:
Received 1 November 2012
Received in revised form
1 December 2012
Accepted 3 January 2013
Available online 16 January 2013

Keywords:
Lithium-ion battery
Tin dioxide
Graphene
One-pot synthesis

ABSTRACT

We report a one-pot hydrothermal approach to synthesize carbon coated-SnO_2/graphene-sheet (SnO_2-C/GNS) nanocomposite. Strong oxidation–reduction reactions to produce GNS by the traditional Hummers' method are avoided. The experiments show that the glucose and tin tetrachloride can intercalate into the thin graphite flake to exfoliate graphite and form SnO_2-C/GNS nanocomposite simultaneously during the hydrothermal process. The approach is quite simple and green. Meanwhile, the prepared SnO_2-C/GNS nanocomposite as an anode material of lithium-ion batteries exhibits higher lithium storage capacity and better cycling performance compared to SnO_2 nanoparticle and SnO_2-C microsphere. It still delivers the reversible capacity of 703 mA h g^{-1} after 80 cycles at a current density of 100 mA g^{-1} and maintains 443 mA h g^{-1} after 100 cycles at a current density of 1000 mA g^{-1}. The improvement in the performance of SnO_2-C/GNS nanocomposite can be attributed to the fully confinement of SnO_2 nanoparticles between the GNS and the carbon layer, which can effectively prevent the detachment and agglomeration of SnO_2 and preserve the integrity of the nanostructure during charge/discharge cycling.

1. Introduction

Tin dioxide (SnO_2) is an attractive anode candidate for the next-generation high-performance lithium-ion batteries. It has a theoretical lithium storage capacity of 782 mA h g^{-1} which is twice as high as that of graphite (372 mA h g^{-1}) [1,2]. However, the practical use of SnO_2-based anodes is hampered by their poor capacity retention arising from the large volume change during charge/discharge processes, which results in the pulverization of active alloy [3]. Recently, SnO_2-based hybrid nanocomposites with controlled size and chemical composition have attracted great attention. One particular interest is nanostructured SnO_2 combined with electronically conductive additives [4–9,14]. The synergistic effects in the composites significantly improve the performance of SnO_2-based anodes.

Graphene, an atomic single layer of honeycomb carbon lattice, has been considered as an ideal supporting material to functionalize the electrode materials in energy conversion and storage due to its superior electronic conductivity, high surface area, flexibility, and good mechanical properties [10–14]. The SnO_2/graphene electrodes exhibited an enhanced cycling performance and higher lithium storage capacity because the graphene nanosheets (GNS) involved can maintain the structural integrity of the electrodes as well as increase the conductivity of the electrodes [10,14,15]. Although many SnO_2/GNS composites have been reported recently, it is worth noting that most of the reported GNS are prepared by the Hummers' method, which usually involves time-consuming

* Corresponding author. Tel.: +1 510 495 2801; fax: +1 510 486 4995.
E-mail addresses: binwang@lbl.gov, edward.bwang@yahoo.com (B. Wang).

0378-7753/$ – see front matter © 2013 Elsevier B.V. All rights reserved.
http://dx.doi.org/10.1016/j.jpowsour.2013.01.025

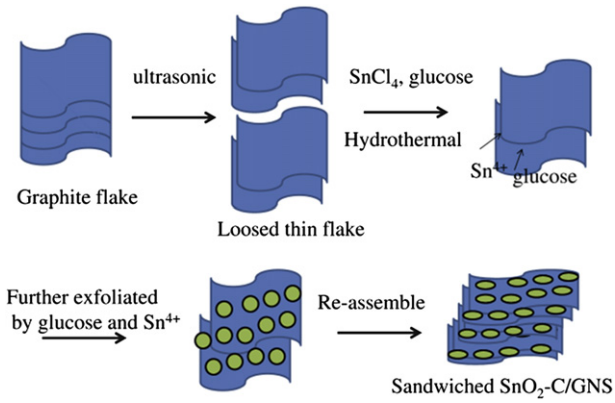

Fig. 1. Illustration of the formation of SnO_2-C/GNS nanocomposite by one-pot hydrothermal reaction.

synthetic procedures and strong oxidation/reduction reagents [10,15–17]. Therefore, it is highly desirable to develop a simple and green chemical route for the synthesis of SnO_2/GNS composite. Furthermore, despite the improvement of SnO_2/GNS anodes, distinct capacity fading in previous reports was still observed. Due to the weak interaction between the SnO_2 nanoparticles and the GNS, it could not effectively slow down the continuous aggregation of SnO_2 nanoparticles that makes them easily peel off from the GNS during lithium insertion/extraction processes. Carbon coating is one of the most utilized ways to improve the cycling performance of SnO_2 anodes. The carbon layer not only serves as a buffer to accommodate the volume changes, but also increases the electronic conductivity of the nanocomposite at the same time [6,7,18–20]. Combining the carbon-coated SnO_2 with the GNS may be an effective way to address the pulverization issue of SnO_2 anode. However, to the best of our knowledge, there is no report about one-pot preparation of the nanocomposite combining the carbon-coated SnO_2 with the GNS.

Herein, we report a simple one-pot approach to synthesize carbon coated-SnO_2/GNS (SnO_2-C/GNS) nanocomposite. In the nanocomposite, SnO_2 nanoparticles encapsulated in carbon shells anchor onto GNS. This kind of nanostructure can effectively prevent the detachment and agglomeration of SnO_2 and preserve the integrity during cycling. Additionally, high conductivity is expected due to the carbon layers making SnO_2 nanoparticles close contact with the GNS.

2. Experimental section

2.1. Material and synthesis

SnO_2-C/GNS nanocomposite was synthesized by hydrothermal and subsequent carbonization process. In a typical process, 15 mg commercial natural flake graphite (KS-6) was dispersed in 15 ml de-ionized water and further dispersed by ultrasonication for 2 h (Microson XL2000). After that, 0.7 g $SnCl_4 \cdot 5H_2O$ (98%, Sigma–Aldrich), and 0.7 g glucose were added to the solution under vigorous stirring. The solution was then transferred into a Teflon lined autoclave and kept at 180 °C for 12 h. After the reaction was stopped, the resulting black solid products were filtrated, washed with distilled water and ethanol to remove the ions possibly remaining in the final products, and dried at 80 °C in air. Finally, the black products were kept in a tube furnace at 450 °C for 3 h under N_2 at a ramping rate of 5 °C min^{-1}. For comparison, SnO_2 nanoparticle was synthesized without using both glucose and graphite under the same condition. SnO_2-C microsphere was synthesized without using graphite under the same condition.

2.2. Characterizations

X-ray diffraction (XRD) patterns were acquired using a Panalytical Xpert Pro diffractometer with monochromatized Cu Kα radiation at a voltage of 45 kV and a current of 40 mA. The scan rate is 0.0005°/s in 0.01° steps. The morphologies were characterized

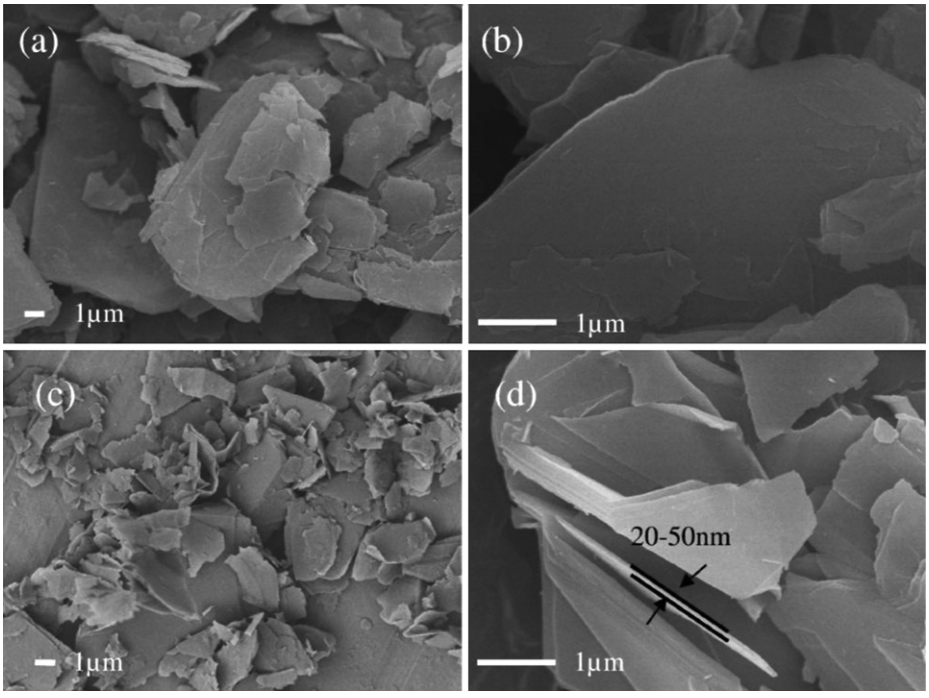

Fig. 2. SEM images of pristine graphite flakes before (a, b) and after ultrasonic treatment (c, d).

using field emission scanning electron microscopy with a voltage of 15 kV (JEOL 7500) and transmission electron microscopy with an acceleration voltage of 200 kV (F20 UT Tecnai microscope). TEM sample was prepared by dispersion of the SnO_2-C/GNS nanocomposite in ethyl alcohol under ultrasonication. The thermogravimetric analysis (TGA Perkin ELEMER TGA7) was carried out at a heating rate of 20 °C min^{-1} from room temperature to 700 °C with airflow. BET measurements were carried out on a Tristar 3000 surface area & porosity analyzer (Micromeritics Instrument Corp.). Degassing process was carried out at 200 °C for 4 h. Raman spectra were collected in the backscattering configuration using a micro-Raman spectrometer (Labram, ISA Groupe Horiba) with a He–Ne laser (632.8, nm, ~0.8 mW at the sample) under the normal atmosphere.

2.3. Electrochemical measurements

The working electrode was prepared by mixing the as-prepared active component with acetylene black and sodium carboxy methyl cellulose (CMC, average Mw: ~250,000, Aldrich) in a weight ratio of 8:1:1. Then the resultant slurry was uniformly casted on pure Cu foil current collector and dried overnight under vacuum. CR2032-type coin cells were assembled in a glove box for electrochemical characterization. The electrolyte was 1 M $LiPF_6$ in a 1:2 mixture of ethylene carbonate and dimethyl carbonate. Li metal foil was used as the counter and reference electrode. The electrochemical performances of the electrode were characterized with an Arbin battery testing system at room temperature. The cells were galvanostatically charged and discharged at different current densities within the range of 0.005–2.0 V. Cyclic voltammograms (CV) were collected at a scan rate of 0.1 mV s^{-1} by a Solartron 1470A working station. The capacity was calculated based on the active material mass.

3. Results and discussion

The fabrication process is illustrated in Fig. 1. Firstly, thick natural graphite flakes are ultrasonically treated to generate loosed thin

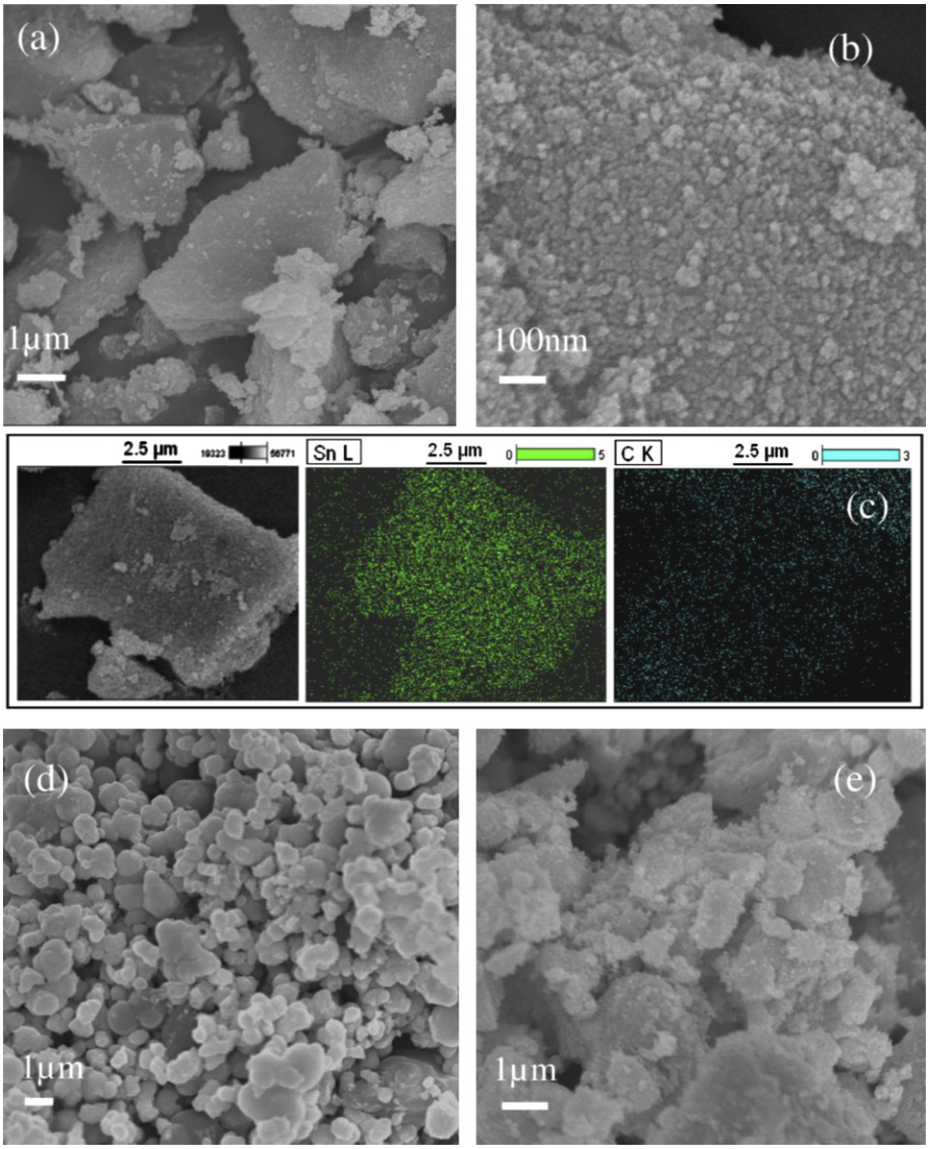

Fig. 3. (a), (b) SEM images of SnO_2-C/GNS nanocomposite at different magnification; (c) SEM image of SnO_2-C/GNS nanocomposite with corresponding EDS maps for Sn and C; SEM images of SnO_2-C microspheres (d) and SnO_2 nanoparticle aggregates (e).

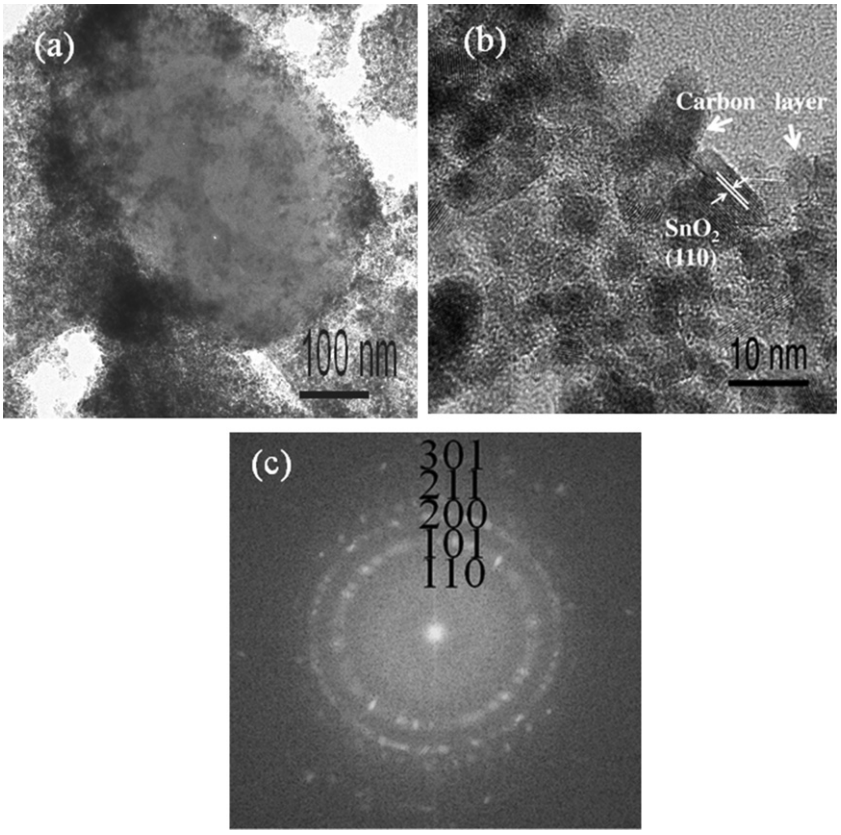

Fig. 4. (a) TEM image, (b) HR-TEM image and (c) its corresponding FFT pattern of SnO_2-C/GNS nanocomposite.

graphite sheets [21]. As shown in Fig. 2, the thick graphite flakes are exfoliated to small parts and some graphene layers are partly peeled off from the edges. Then, in hydrothermal condition, the glucose and Sn^{4+} intercalate into the loosed thin graphite sheets to further exfoliate graphite and to generate graphene sheets. Carbon coated SnO_2 nanoparticles are formed by hydrolysis of stannate and subsequent deposition of glucose-derived carbon-rich polysaccharide. The carbon coated SnO_2 nanoparticles simultaneously anchor on the GNS layers and act as nucleation sites for further particle growth [15,22]. Finally, sandwich-liked SnO_2-C/GNS nanocomposite is achieved by stacking and interlocking of individual sheets under a filtration-induced directional flow [23,24].

The morphology, structure, and composition of the SnO_2-C/GNS nanocomposite are further examined by SEM (scanning electron microscopy) and TEM (transmission electron microscopy). Large sandwich-liked plates can be observed in SEM image (Fig. 3a).

As revealed by the high-magnification SEM (Fig. 3b), numerous nanoparticles with the size of 10–20 nm can be clearly observed on the surface of these plates. The energy-dispersive X-ray spectrum (EDS) elemental mapping is used to determine the component of the composites. From the elemental distribution of tin and carbon in Fig. 3c, it can be known that the SnO_2 particles are uniformly distributed in the carbon matrix. However, only micron-sized SnO_2-C spheres formed in the similar synthesis conditions without using graphite as a substrate (Fig. 3d) and only SnO_2 nanoparticle aggregates formed in the absence of both glucose and graphite (Fig. 3e). The formation of such sandwich-liked plates implies the successful growth of SnO_2-C nanoparticles on the GNS. TEM image in Fig. 4a reveals that the SnO_2 particles are supported by GNS layers in the SnO_2-C/GNS nanocomposite. Besides, thin layer of carbon can be found surrounding the SnO_2 particles from HR-TEM image in Fig. 4b (indicates by the arrows). Fig. 4c shows the corresponding FFT pattern of the HR-TEM image. The Raman spectrum of SnO_2-C/GNS nanocomposite also demonstrates the existence of carbon, graphene and SnO_2 nanoparticle in the SnO_2-C/GNS nanocomposite [25]. As shown in Fig. 5, two typical carbon peaks at about 1355 cm^{-1} (D band) and 1597 cm^{-1} (G band) are observed. Meanwhile, three peaks can be observed at 472, 631 and 774 cm^{-1}, corresponding to E_g, A_{1g} and B_{2g} vibrations of the SnO_2 nanoparticles. The intensity ratio of the D band to the G band, I_D/I_G, of SnO_2-C/GNS is calculated as 0.26, which is higher than those of

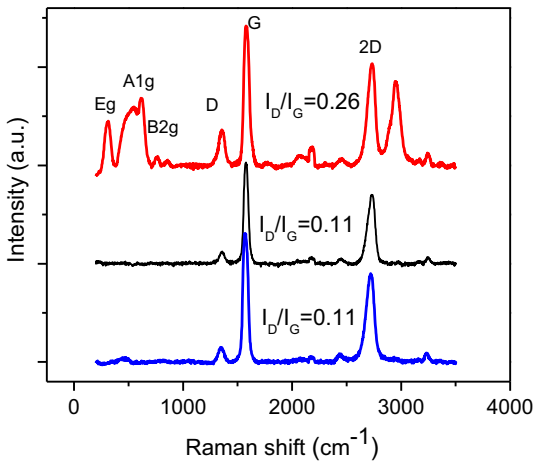

Fig. 5. Raman spectra of graphite flakes (blue), thin graphite flakes after ultrasonification (black) and SnO_2-C/GNS nanocomposite (red). (For interpretation of the references to color in this figure legend, the reader is referred to the web version of this article.)

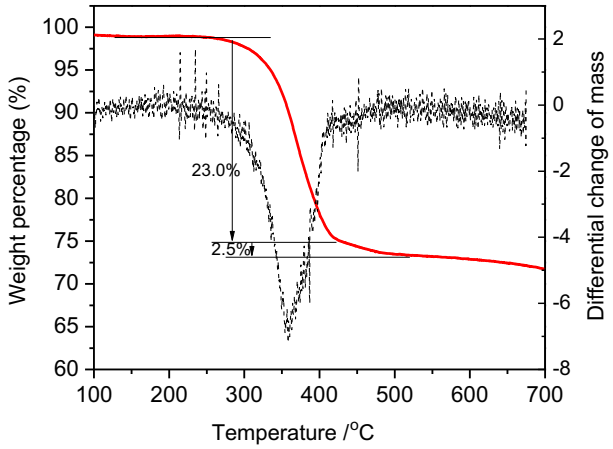

Fig. 6. Thermogravimetric analysis and its differential curve of SnO_2-C/GNS nanocomposite.

graphite flakes (0.11) and thin graphite flakes (0.11). The obviously enhancement of the intensity ratio in the SnO_2-C/GNS nanocomposite can be attributed to the carbon coating and the increase of the disorder in the graphene resulting from aggressive hydrothermal reaction and the SnO_2 nanoparticles loading. The total carbon content (the GNS and the carbon resulting from carbonization of glucose) was determined by TGA (Fig. 6). The TGA curve of the SnO_2-C/GNS nanocomposite displays two distinct regions of weight loss. The initial weight loss between 300 and 400 °C is mainly due to the removal of amorphous carbon layer resulting from carbonization of glucose, while the weight loss in the second region (400–500 °C) could be attributed to the removal of GNS, since GNS is more thermally stable than amorphous carbon.

The crystallographic structure of the product was characterized by XRD measurement (Fig. 7a). All of the diffraction peaks can be indexed to tetragonal SnO_2 with cassiterite structure (JCPDS Card No41-1445). It is difficult to identify GNS peaks in the powder diffraction pattern due to its low content as determined by TGA. Besides, the (110) peak of the tetragonal SnO_2 overlapped with the (002) peak of the graphene that makes it hard to distinguish the GNS diffraction peak. The average crystallite size of SnO_2 is about 8.0 nm calculated by using Scherrer's equation based on XRD, which is well consistent with TEM results. To further investigate the surface area and pore size of the sample, nitrogen isothermal adsorption technique was used. Nitrogen adsorption/desorption isotherms in Fig. 7b exhibit a hysteresis typical of a nanoporous system [16,26,27]. According to Brunauer–Emmett–Teller (BET) analysis, the total specific surface area is 164 $m^2\ g^{-1}$. The average Barrett–Joyner–Halenda (BJH) pore size distribution displays a unimodal peak of around 12 nm.

It is well known that the electrochemical performance is closely related to the material nanostructures. The SnO_2-C/GNS nanocomposite has two different kinds of carbon buffering-glucose-carbonized carbon layer and GNS layer, leading to the enhanced lithium storage properties. The electrochemical process of the SnO_2 anode contains many steps, which has been exhaustively elucidated by Sandu [28,29]. It is generally accepted that the electrochemical process of SnO_2 anodes can be simplified to two principal reactions:

$$SnO_2 + 4Li^+ + 4e^- \rightarrow 2Li_2O + Sn \quad (1)$$

$$Sn + xLi^+ + xe^- \leftrightarrow Li_xSn (0 \le x \le 4.4) \quad (2)$$

To identify the electrochemical process, CV measurement was performed as shown in Fig. 8a. Two well-defined cathodic peaks at 0.7 V and 0.1 V are observed in the first cycle. The peak at 0.7 V corresponds to the solid electrolyte interface (SEI) formation and the reductive transformation of SnO_2 to Sn. While the one at 0.1 V can be attributed to the formation of alloy as described by reaction (2). Two corresponding anodic peaks are observed. One is at about 0.6 V, which can be attributed to dealloy of Li_xSn alloy. The other peak is at about 1.25 V, which may correspond to partial reversibility of reaction (1) [18,30]. The anodic peak position and the intensity are fare stable for the second and following cycles, indicating the good electrochemical stability. Fig. 8b shows a typical discharge–charge voltage profile of SnO_2-C/GNS nanocomposite anode for the first and second cycles at a current density of 100 mA g^{-1}. The initial charge and the discharge capacity are 1058 and 1764 mA h g^{-1}, respectively. The capacity loss in the first cycle is mainly attributed to the initial irreversible formation of Li_2O, electrolyte decomposition and formation of SEI layer, which is in good agreement with CV testing results. To highlight the superiority of the SnO_2-C/GNS nanocomposite as an anode material of lithium-ion batteries, we compared its electrochemical performance with those of SnO_2 nanoparticle and SnO_2-C microsphere. Fig. 8c shows the comparative cycling performance of SnO_2-C/GNS nanocomposite and the other two counterparts at a current density of 100 mA g^{-1}. It is apparent that the as-prepared SnO_2-C/GNS nanocomposite demonstrates much better electrochemical performances compared to the other two samples, in terms of both lithium storage capability and cyclic capacity retention. The

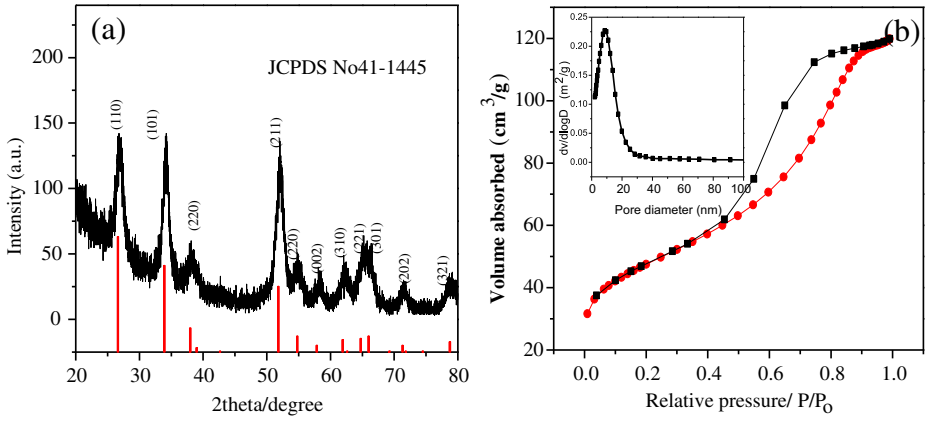

Fig. 7. (a) XRD pattern and (b) nitrogen adsorption and desorption isotherm (inset: pore size distribution) of SnO_2-C/GNS nanocomposite.

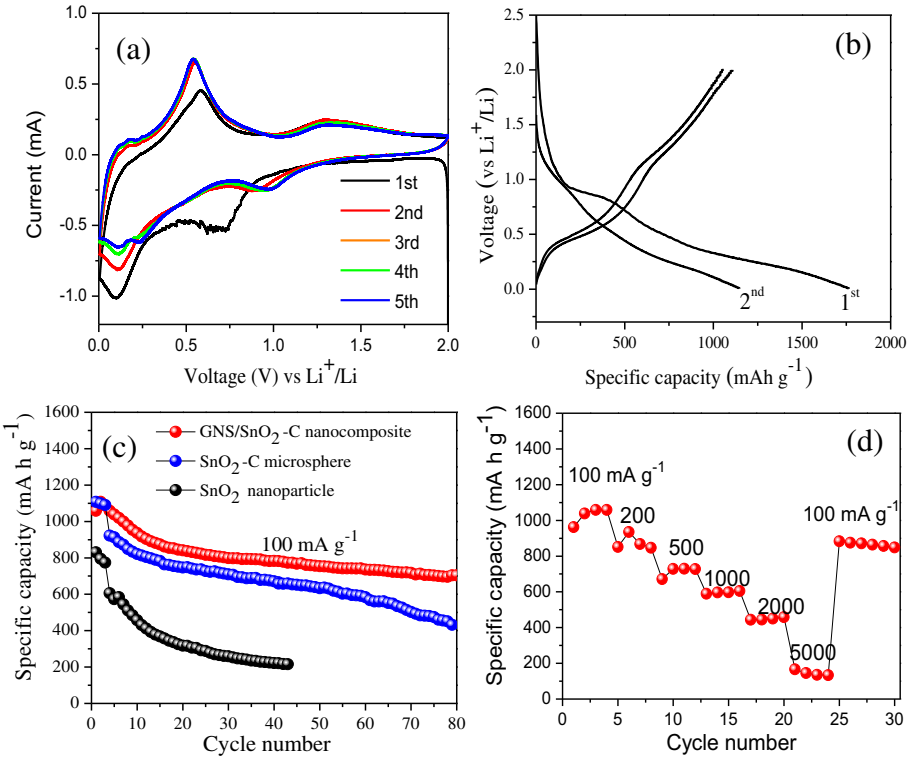

Fig. 8. (a) Cyclic voltammograms of SnO_2-C/GNS nanocomposite electrode at a scan rate of 0.1 mV s^{-1}; (b) Charge–discharge profiles for the first two cycles of SnO_2-C/GNS nanocomposite electrode; (c) Cycling performance of SnO_2 based anodes at a current density of 100 mA g^{-1}; and (d) rate capability of SnO_2-C/GNS nanocomposite electrode. (The line appearing in Fig. 8(c) and (d) is a mere guide to the eye.).

SnO_2-C/GNS nanocomposite electrode manifests excellent capacity retention and high reversible capacity. After 80 cycles, it still delivers the charge capacity of 703 mA h g^{-1} with the retention of 67% of initial reversible specific capacity, corresponding to about 90% theoretical specific capacity of SnO_2 (782 mA h g^{-1}). The SnO_2-C microsphere anode shows the second-best performance owing to the carbon buffer effect. It maintains a charge capacity of 432 mA h g^{-1} after 80 cycles with the retention of 39.2% of initial value. Without any buffer layer, the capacity of SnO_2 nanoparticle fades quickly to a value of 300 mA h g^{-1} in less than 20 cycles, below the theoretical capacity of graphite (372 mA h g^{-1}). Meanwhile, it should be pointed out that the cycling performance of SnO_2-C/GNS nanocomposite anode is better than those of SnO_2-C [18,20], SnO_2-graphene [14], and SnO_2-CNT [5,8,9,14,31] at the same current density. To further investigate the electrochemical performance of the SnO_2-C/GNS nanocomposite, the rate capability was measured as shown in Fig. 8d. The SnO_2-C/GNS nanocomposite electrode also illustrates a good rate performance at different current densities: 100, 200, 500, 1000, and 5000 mA g^{-1}. It should be noted that when the current density return to the low current density of 100 mA g^{-1}, the SnO_2-C/GNS nanocomposite electrode still delivers a high charge capacity of about 849 mA h g^{-1}, which means the integrity of the nanocomposite electrode has been well maintained even after cycling at high charge/discharge current densities. For practical application, the battery material is required to have long cycling life even at high current density. So we also evaluated the long life cycling performance of the SnO_2-C/GNS nanocomposite anode at a high current density of 1000 mA g^{-1}. As shown in Fig. 9a, it exhibits a high charge capacity of 443 mA h g^{-1} after 100 cycles with the retention of 62% of initial value. At the

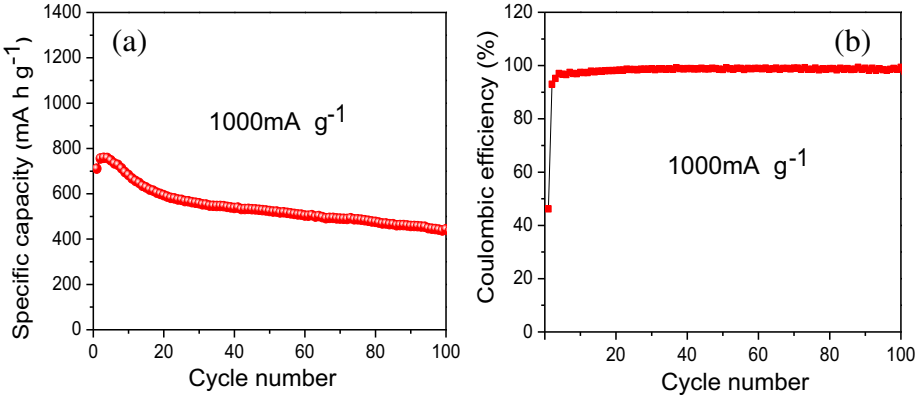

Fig. 9. (a) Cycling performance and (b) Coulombic efficiency of SnO_2-C/GNS nanocomposite at a current density of 1000 mA g^{-1}.

same time, the Coulombic efficiency keeps steadily with an average value of 99% (Fig. 9b).

4. Conclusion

In summary, we developed a simple one-pot method for preparation of the SnO_2-C/GNS nanocomposite in combination of carbon coated SnO_2 with the GNS. This method is based on hydrothermal treatment of tin tetrachloride, glucose and loosed graphite flake in water. Strong oxidation and reduction reactions to produce GNS by the traditional Hummers' method are avoided. The as-prepared SnO_2-C/GNS nanocomposite exhibits higher lithium storage capacity and better cycling performance compared to SnO_2 nanoparticle and SnO_2-C microsphere. It still delivers the reversible capacity of 703 mA h g^{-1} after 80 cycles at a current density of 100 mA g^{-1} and delivers 443 mA h g^{-1} after 100 cycles at a current density of 1000 mA g^{-1}. From these results, it can be seen that the SnO_2-C/GNS nanocomposite is a promising anode material for high-performance lithium-ion batteries. This simple and green approach may be extended to the fabrication of other carbon coated metal oxide/GNS nanocomposites to address the issues in energy storage field.

Acknowledgment

The authors acknowledge support of the National Center for Electron Microscopy, Lawrence Berkeley Lab, which is supported by the U.S. Department of Energy under Contract # DE-AC02-05CH11231.

References

[1] L. Ji, Z. Lin, M. Alcoutlabi, X. Zhang, Energy Environ. Sci. 4 (2011) 2682.
[2] D. Deng, M.G. Kim, J.Y. Lee, J. Cho, Energy Environ. Sci. 2 (2009) 818.
[3] W.J. Zhang, J. Power Sources 196 (2011) 13.
[4] D.W. Kim, I.S. Hwang, S.J. Kwon, H.Y. Kang, K.S. Park, Y.J. Choi, K.J. Choi, J.G. Park, Nano Lett. 7 (2007) 3041.
[5] Z. Wen, Q. Wang, Q. Zhang, J. Li, Adv. Funct. Mater. 17 (2007) 2772.
[6] X. Wang, X. Zhou, K. Yao, J. Zhang, Z. Liu, Carbon 49 (2011) 133.
[7] B. Zhang, X. Yu, C. Ge, X. Dong, Y. Fang, Z. Li, H. Wang, Chem. Commun. 46 (2010) 9188.
[8] L. Noerochim, J.Z. Wang, S.L. Chou, H.J. Li, H.K. Liu, Electrochim. Acta 56 (2010) 314–320.
[9] Z. Wang, G. Chen, D. Xia, J. Power Sources 184 (2008) 432.
[10] C.F. Zhang, X. Peng, Z.P. Guo, C.B. Cai, Z.X. Chen, D. Wexler, S. Li, H.K. Liu, Carbon 50 (2012) 1897.
[11] L.W. Ji, Z.K. Tan, T. Kuykendall, E.J. An, Y.B. Fu, V. Battaglia, Y.G. Zhang, Energy Environ. Sci. 4 (2011) 3611.
[12] A. Bhaskar, M. Deepa, T.N. Rao, U.V. Varadaraju, J. Power Sources 216 (2012) 169.
[13] J. Yao, X.P. Shen, B. Wang, H.K. Liu, G.X. Wang, Electrochem Commun. 11 (2009) 1849.
[14] S.M. Paek, E. Yoo, I. Honma, Nano Lett. 9 (2009) 72.
[15] C.H. Xu, J. Sun, L. Gao, J. Mater. Chem. 22 (2012) 975.
[16] B.J. Li, H.Q. Cao, J.X. Zhang, M.Z. Qu, F. Lian, X.H. Kong, J. Mater. Chem. 22 (2012) 2851.
[17] D.A.C. Brownson, D.K. Kampouris, C.E. Banks, J. Power Sources 196 (2011) 4873.
[18] X.W. Lou, J.S. Chen, P. Chen, L.A. Archer, Chem. Mater. 21 (2009) 2868.
[19] N.H. Zhao, G.J. Wang, Y. Huang, B. Wang, B.D. Yao, Y.P. Wu, Chem. Mater. 20 (2008) 2612.
[20] P. Wu, N. Du, H. Zhang, J. Yu, Y. Qi, D. Yang, Nanoscale 3 (2011) 746.
[21] H.M. Liu, W.S. Yang, Energy Environ. Sci. 4 (2011) 4000.
[22] H.L. Wang, J.T. Robinson, G. Diankov, H.J. Dai, J. Am. Chem. Soc. 132 (2010) 3270.
[23] C.Y. Wang, D. Li, C.O. Too, G.G. Wallace, Chem. Mater. 21 (2009) 2604.
[24] H. Chen, M.B. Muller, K.J. Gilmore, G.G. Wallace, D. Li, Adv. Mater. 20 (2008) 3557.
[25] C. Zhong, J.Z. Wang, Z.X. Chen, H.K. Liu, J. Phys. Chem. C 115 (2011) 25115.
[26] M.Y. Cheng, B.J. Hwang, J. Power Sources 195 (2010) 4977.
[27] B. Wang, J.L. Cheng, Y.P. Wu, D. Wang, D.N. He, Electrochem Commun. 23 (2012) 5.
[28] I. Sandu, T. Brousse, D.M. Schleich, M. Danot, J. Solid State Chem. 177 (2004) 4332.
[29] I. Sandu, T. Brousse, D.M. Schleich, M. Danot, J. Solid State Chem. 179 (2006) 476.
[30] R. Demir-Cakan, Y.S. Hu, M. Antonietti, J. Maier, M.M. Titirici, Chem. Mater. 20 (2008) 1227.
[31] P. Wu, N. Du, H. Zhang, J.X. Yu, D.R. Yang, J. Phys. Chem. C 114 (2010) 22535.